Physical-Model-Aided Antenna Pattern Calibration for Flight Inspection

[1]Matthew Gilliam, [1]Yan (Rockee) Zhang, and [1]John Dyer

[1]Intelligent Aerospace Radar Team (IART)
School of Electrical and Computer Engineering
University of Oklahoma,
Norman, OK 73019

The calibration and inspection of various antennas related to navigation, aviation and flight operations has been a big challenge for agencies such as FAA and DoD. These antennas include both ground and airborne components. Antenna systems at ground infrastructure include navigational aide systems such as VOR/LOC, TACAN/DME, and Glide Slope, and include the ground-based surveillance radars. The antennas mounted on the aircraft include various aviation probe antennas and airborne radars. The flight inspection mission requires precise measurement of signal power at locations around any facility. Calibration of airborne radar antenna mounted on aircraft is also needed for precise radar functions. The difficulties, however, lie in the fact that the aircraft body and the environment have significant impacts on the signal measurement quality, which is usually difficult to characterize. This work focuses on how the airframe affects the typical aviation antenna measurements, and a possible way to "normalize" such impacts to gain the desired "effective" radiation patterns. We mainly reply on computational electromagnetic (CEM) tools to establish the physical scattering model of the aircraft with respect to different simplified antenna models, and then validate the radiation patterns through actual flight test data collections. Initial comparisons between the simulations and flight measurements reveal some interesting behaviors of radiation patterns on the aircraft installations, further issue of electromagnetic compatibility in the complex aircraft operations, and the potential of using unmanned aerial systems (UAS) to automate the measurement procedure in the future.

1. INTRODUCTION

Military and civilian aviation support require accurate calibration of navigational aide signals, as these navigational supports requires precise calibrations. For example, ICAO required 3 dB accuracy of signal-strength (SS) measurements for aviation flight inspections. Precise measurement of signal strength is important to determine the coverage. This includes VOR/LOC, TACAN/DME, and Glide Slope (GS) transceivers. Despite the latest development of flight inspection instrumentations, the significant challenges of such accurate calibrations still exist, such as:

(1) Originally, the majority of the navigational antennas on the aircraft are designed to be onmi-directional. However, the scattering and interaction between navigational signals (which are from VHF to L band) and aircraft body cause radiation pattern distortions. Such distortions become more severe when the aircraft is larger (which is the case of the current flight inspection aircraft). Also, such distortions have variations (sometimes more than 20 dB) across a small span of spatial angles, which is also aircraft-dependent and test-environment-dependent. Some instrumentation vendors attempted to "compensate" such variations as part of calibration, but only provide "gain normalization factor" for very coarse angle intervals.

(2) Cost of inspection and validation, as well as personnel training to support the validation and inspection is very high. Currently, each inspection flight involves coordination among control towers, ground stations, and the flight crews. The aircraft are large and expensive to operate, and even so, the quality and quantity of signal sample collection are limited sometimes. The mutual couplings among different antennas also constitute electromagnetic compatibility (EMC) problems.

(3) A similar situation exists for other onboard sensor systems. For the RF sensor systems that need precise radiation patterns, such as airborne radars, the interactions between the airframe and antennas affect many aspects of their applications. The technology being investigated in this work is also applicable to the radar sensor radiations and calibrations.

To address these challenges, previous studies have initiated efforts to establish a combined modeling and measurement approach for aircraft antenna characterizations [4-6]. Concepts of using unmanned aerial system (UAS) for navigational signal inspections are also mentioned in recent literature [7,8]. These efforts mainly use chamber measurement for validation, and there are no sufficient validations to show the quality of the calibration data or software-defined receivers (SDR), in term of matching the quality of existing flight inspection instruments used in large aircraft.

Recently, we worked together with FAA flight inspection (FI) and industry to investigate the feasibility of developing a combination of computational electromagnetics (CEM) model for the navigational aide signal slight inspections. We also combine the CEM model with new RF sensing solutions, including unmanned aerial system (UAS) and software-defined radio (SDR). For the first time, we use actual flight inspection instrumentation and tests to validate the EM simulations. We also developed a simplified antenna modeling procedure, which showed promise to achieve a compromise between model complexity and accuracy and demonstrated its effectiveness. The long-term plan for the future of flight inspection is illustrated in Figure1. In this plan, the flight inspection probe will use a single antenna and a "universal" radio receiver, instead of separated antennas for different transponders. Similarly, ground stations will also use unified transmitters. The inspection flight data will be combined with CEM data in the calibration process.

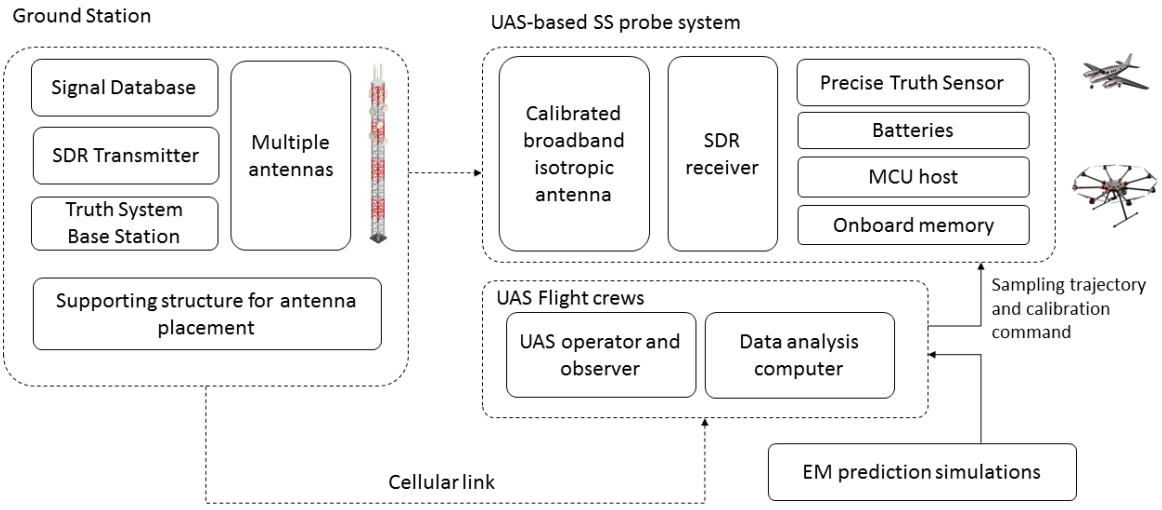

Figure 1: The proposed new flight inspection scheme and solution based on UAS and software-defined radio systems.

The benefits of using UAS platforms for the FI mission are clear – currently, small to medium UAVs can reach most of the Class-G airspace altitude and required airspace coverage from FI. Cost-saving from operating large inspection aircraft and flights will be tremendous, training of flight crew will also be much simpler. Another important benefit is that as the UAS size is much smaller than the wavelengths of navigational radios, the effect of multiple scattering will be less of a problem, which means we may expect the antenna patterns are more isotropic than those from larger aircraft, which makes it easier for calibration using CEM pattern base.

Even though, there are still obstacles to overcome before the UAS-based FI calibration becomes a reality. First, the payload instrumentation on the UAS will need to have much smaller size and weight than currently certified measurement systems, while the requirements for precisions are not reduced. Second, as the UAS flying mostly in low altitude, environment (such as ground multipath) will still have impacts on radiation patterns. Third, due to battery life limit, the data can be collected and stored on the current UAS platforms are still limited. In this stage, our strategy is still focusing on the calibration of antennas on the manned aircraft first, then the experience accumulated can be applied to UAS platforms as well. In addition, as we mentioned earlier, the same techniques and procedures can be applied to airborne radar antennas as well.

Figure 2 shows the current installations of FI antennas on a manned aircraft (CL-605 jet). As can be seen, different navigational antennas and avionic antennas are located at different places on the body, and some of them are close to each other. The DME antennas are the belly more subjective to scattering from the aircraft body (such as landing gear).

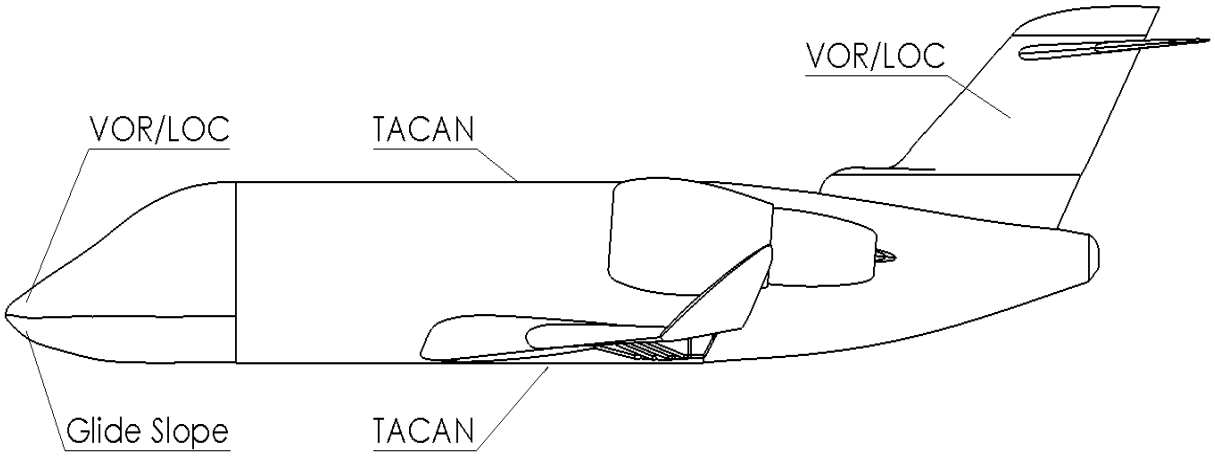

Figure 2: Illustration of how the relevant navigational antennas are installed on a CL-605 flight inspection aircraft.

2. ESTABLISHMENT OF PHYSICAL MODELS

2.1 Aircrafts

We used a combination of 3D laser scanning and manual edit of existing CAD models to create the 3D computational models for the aircraft. Figure 3(a) shows an STL model created from a 3D laser scan of King Air inspection aircraft, which is imported into the FEKO environment. Figure 3(b) shows the meshed Challenger Jet aircraft model, which is imported into a CST Studio environment. The key to creating the models is to balance fidelity and complexity. The laser scanned models are most accurate but contain too many unnecessary details, and it cannot be used for EM simulation environment directly. On the other hand, the general CAD models would not contain enough details on some parts. Therefore, we used a laser scan model as a basis, measured aircraft wing structure dimensions, and combined these in modifying generic CAD models. At the radio frequencies, these models can reasonably represent the key features of the aircraft structures.

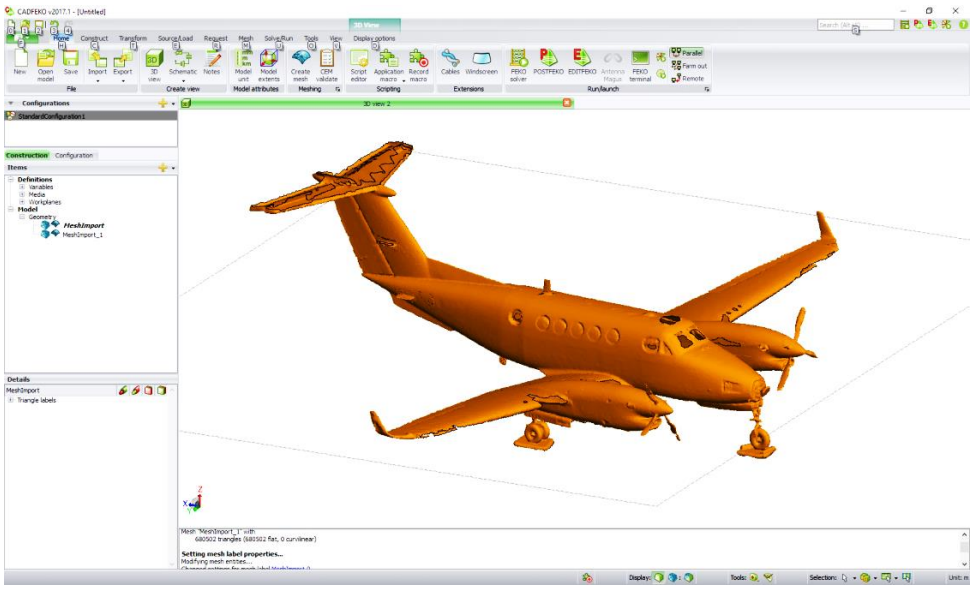

(a)

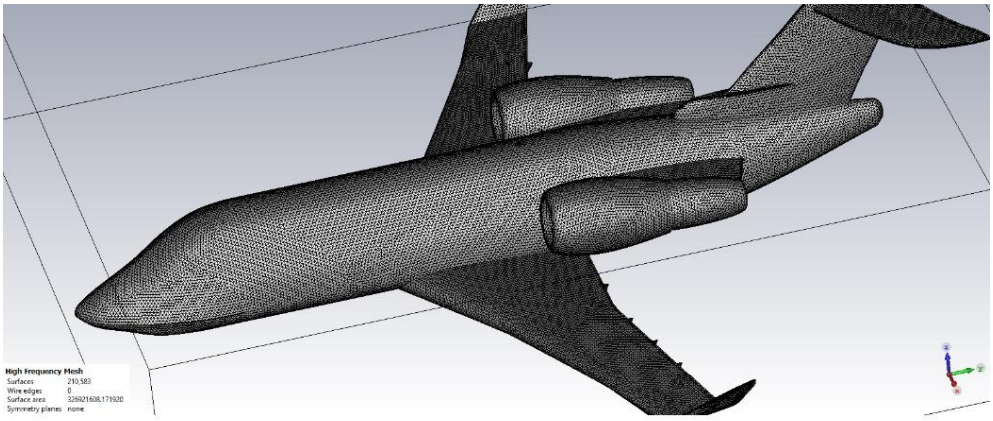

(b)

Figure 3: 3D aircraft structure modeling for the CEM. (a) 3D model of King-Air using 3D laser scanning, (b) Meshed Challenger Jet model.

2.2 Antennas

Table 1 lists the main antennas that need to be modeled and the frequency bands they cover. Samples of each of these antennas are obtained from FAA and tested for both radiation patterns and S-parameters (shown in Figure 4). Characterization of these antennas provides references for "behavior models" even the detailed designs of them are not available.

Table 1: The basic list of navigational flight inspection antennas

Antenna functions	Antenna mounting locations	Aircraft	Freq Range	Modeling Method
VOR/LOC	Tail	BE-300PL	108-118 MHz,	Simplified monopole

			11 steps	
VOR/LOC/GBAS	Tail and nose	CL-604/5	108-118 MHz 11 steps	Simplified monopole
TACAN/DME	Top and bottom	BE-300PL	960-1215 MHz 51 steps	BASIC: Simplified monopole at belly location, IMPROVED: full annular ring slot model
Glideslope (GS) antenna	Nose	BE-300PL	328-336 MHz 7 steps	Simplified monopole at nose
Glideslope (GS)	Nose	CL-604/5	328-336 MHz, 7 steps	Simplified monopole at nose
TACAN/DME	Top and bottom	CL-604/5	960- 1215 MHz, 51 steps	BASIC: Simplified monopole at belly location, IMPROVED: Blade antenna model (on-development)

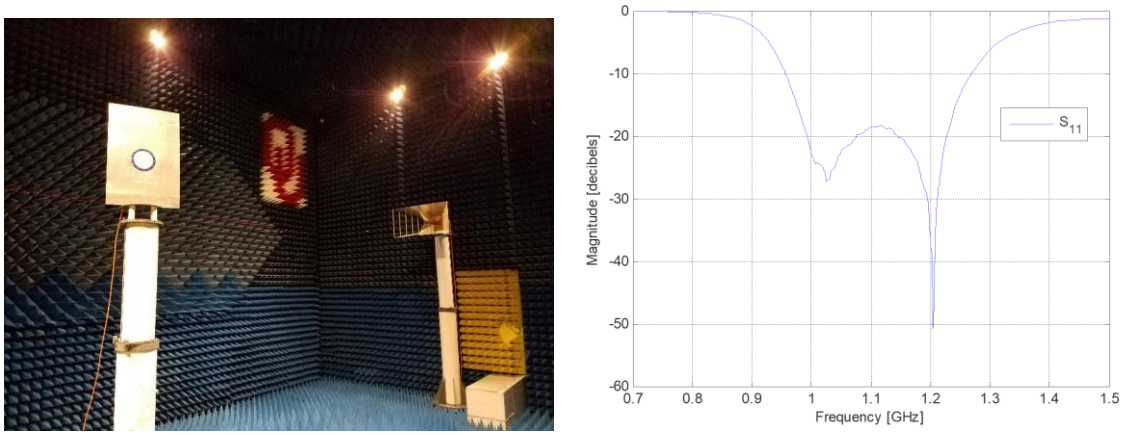

(a) **(b)**

Figure 4: Characterizing of actual aviation antennas. (a) chamber pattern measurement (DME antenna), (b) Lab measurement of the antenna port return loss (DME antenna).

The measured antenna patterns clearly show identical patterns to ideal dipole or monopole. Therefore, using simple dipole or monopole antenna elements to model these antennas are justified. However, there are additional complexities. The first issue is that the dipole elements usually do not support the wideband or multiband operations (such as in Figure 4(b)). So, there will be strong variation of radiation field strength over frequencies if a single dipole is used. The second issue is spatial variation is sometimes caused by destructive body scattering, while in other time caused by numeric errors. Additional model elements are also needed to take account into the "unexplained" blockage effect during actual flight measurements.

As a result, the procedure flow in Figure 5 was developed for antenna modeling. First, we confirmed the required frequency band coverage, and the "nominal" radiation patterns (such as basic monopole) for each frequency, from initial lab tests. Second, we generate simple dipole/monopole models at different frequencies, adding blockage element models based on the observed "blockage zones" in previous measurement observations. Next, we place the antenna models at the aircraft installation positions. Simulation runs are performed for all the frequencies. The results are examined based on frequency domain gain requirement model (based on antenna specification sheet) and spatial smoothness assumptions (which is based on empirical experience). The optional step next is to do data smoothing in frequency and spatial domain to match to actual antenna gain and VSWR over frequencies and specific spatial angles.

The pattern data, after these procedures, are stored in CSV data files that allows access and usage from flight inspection software.

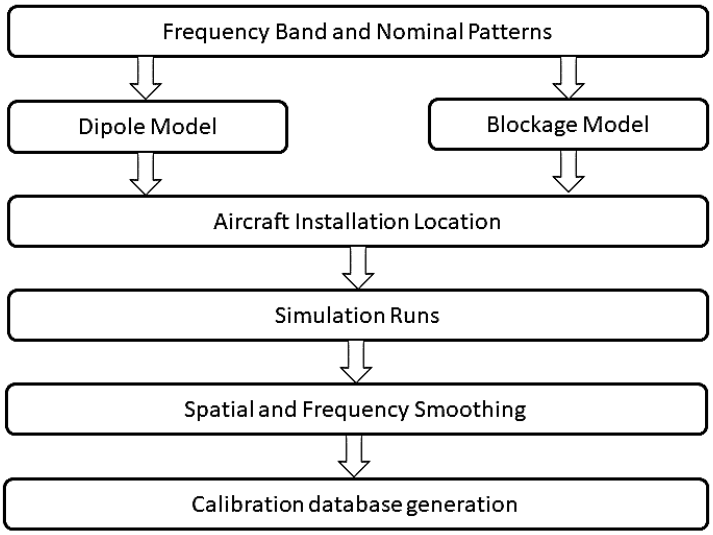

Figure 5: Procedures of pattern simulations and calibration dataset generation.

The above data product generation procedure still has limitations, for example, it cannot incorporate the effects of RF signal paths to instruments. Complex RF channels and networks throughout the aircraft are expected, and sometimes they cause strong variations. Also, the actual navigational signals are AM/PM modulated waveforms while CEM can only assume CW waveforms. Environmental multipaths and scattering are not considered. Nevertheless, the model can provide the "first step" toward the final goals in the Section I.

3. SIMULATION PROCESS

The simulation environment is described in Table 2. MLFMM solver from CST Studio was selected for the solver solution due to the numeric stability and being user friendly. Each run of the simulation covers one frequency point and one aircraft configuration (determined by the state of landing gear and flap), which takes 1-10 hours of run time depending on the configuration of the solver (such as precision requirement, memory requirement).

Table 2: Basic simulation configurations

CEM tool	CST Studio Suite
EM solver	Multi-level Fast Multipole (MLFMM)
Aircraft materials	Assumed to be PEC (perfect electric conductor)
Antennas	Modeled using the procedure in Section 2.2
Workstation	Intel I-7 6950X@3GHz, 64 GB RAM
Run-time	1-10 hours for each frequency point and each aircraft configuration

Figure 6 shows examples of 3D pattern outputs for the King Air system. Such 3D patterns are further processed in MATLAB following the procedures in Figure 5. The MATLAB programs sort the pattern results belonging to

different antennas, perform coordinate transformations, and storing into the calibration database. The database then contains 3D radiation strength values in dB with one-degree spatial resolution.

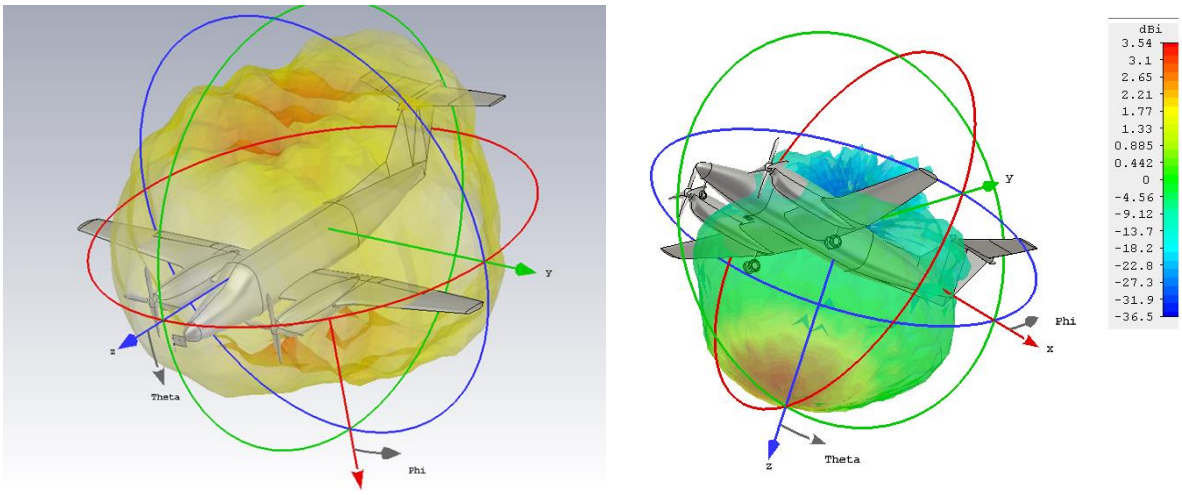

(a) **(b)**

Figure 6: Example of 3D pattern simulations (for King Air system model), (a) VOR-LOC, (b) DME-bottom.

4. VALIDATION PROCESS

4.1 Coordinates and Test Data Collection

Flight measurement is an expensive procedure so only limited validations are done at this stage. Most of the light data collections are from the "in-flight" configurations, which contains no landing gear and has a specific flap angle. The "low-resolution" validation measurement data is available from Spring 2018, which include data collected from both King Air and CL-605 flight, in the same horizontal plane (-1 deg elevation angle), and measurement resolution is 30 degrees. The high "high resolution" validation measurement data is available since Nov 2018, which only includes data from King Air, and the angular resolution is between 10 to 20 degrees. The "high resolution" data also contains multiple elevation angles.

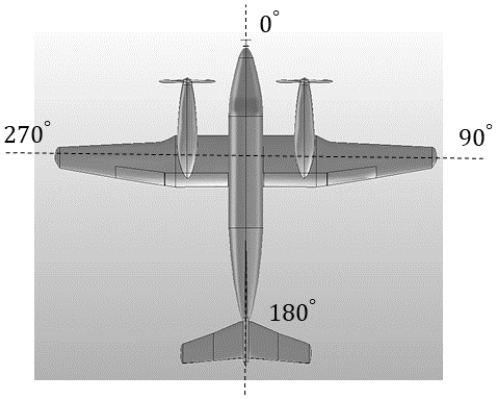

Figure 7: Aircraft coordinate system.

The 3D pattern data was first converted to the aircraft coordinate system as shown in Figure 7. Note the elevation angle is defined as growing positive when going "up" from the nose direction. The measured signal strength patterns are converted to "antenna radiation patterns" which are based on the antenna-centered coordinates.

4.2 Low-resolution measurement data

Figure 8 shows examples of the comparisons between simulated and measured navigational radiation patterns for the "low-resolution measurement data". The measurements show reasonable agreements. Because the measurement resolution is low, we do not calculate dB accuracy comparisons. It is noted that at some angles the model output pattern has deep nulls while the measurements do not have. It is believed that these nulls are reasonable due to the dipole blockage by the aircraft tails, while actual RF measurement instruments may have "smoothing" done in certain ways. Further "smoothing" of these patterns at data processing will help to improve the matching to the measurements.

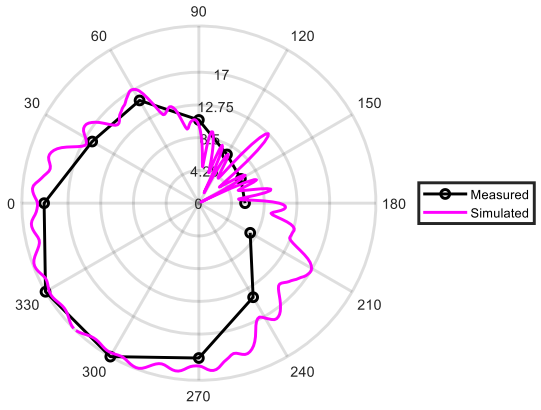

(a)

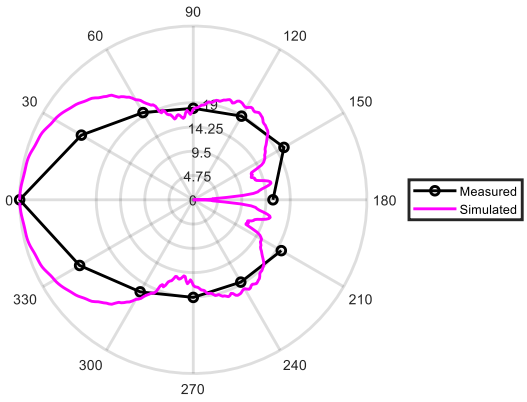

(b)

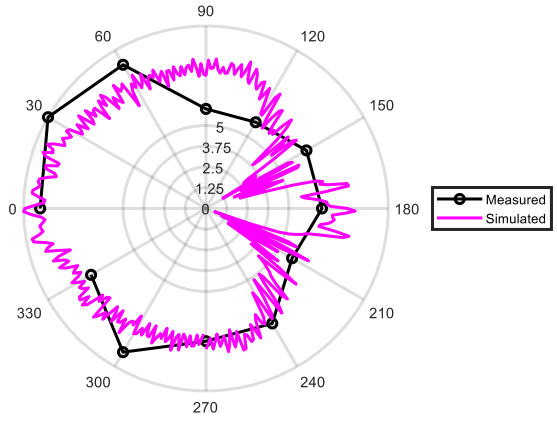

(c)

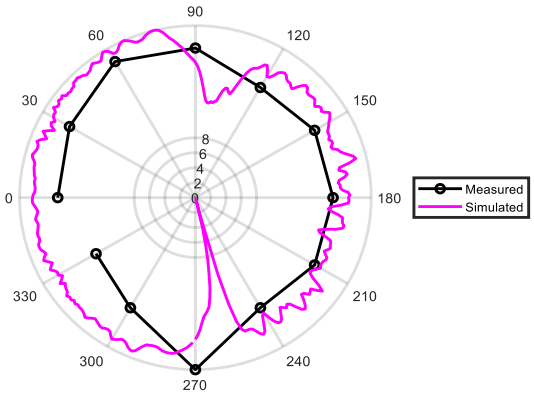

(d)

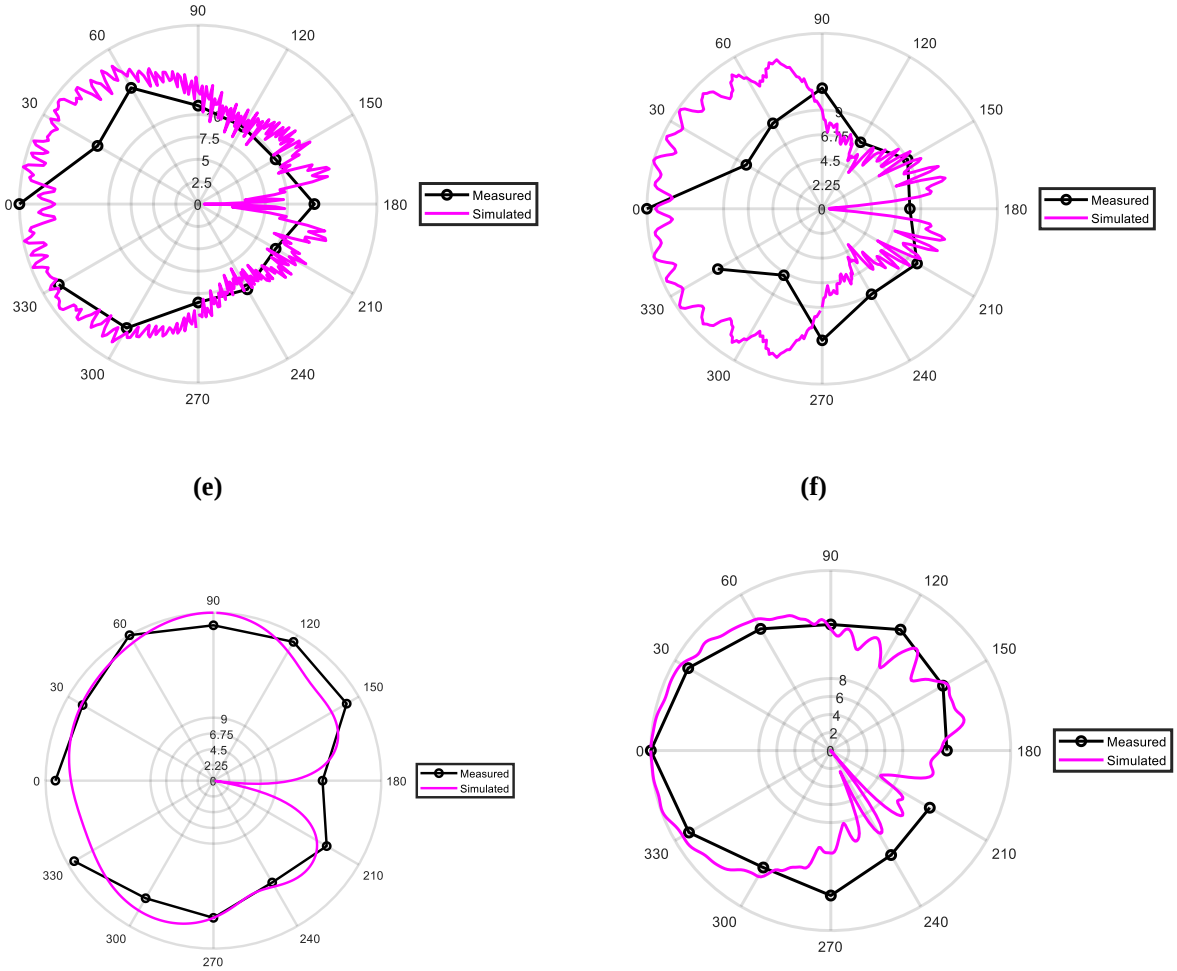

Figure 8: Comparing the unsmoothed EM simulation output with flight test measurement for the low-resolution measurement data, at specific measurement frequencies and in the aircraft coordinates (for "in flight" configuration). To save space, the figures only show some example results. (a) GS-1 antenna for King Air. (2) GS-1 antenna for CL-605. (c) TACAN-DOWN for King Air, (d) TACAN-bottom for CL-605. (e) TACAN-TOP for King Air, (f) TACAN-TOP for CL-605. (g) VOR-1 at the tail of King AIR, (h) VOR-Forward at the nose of CL-605.

4.3 High-resolution measurement data

For "high-resolution measurements", we compare the simulation and measurement patterns at each sampling directions, and then obtain more accurate error statistics. In Figure 9, we use the red color labels to tell the exact elevation angle from each measurement point. For the four examples shown here, three of them can achieve the error standard deviation of less than 3 dB. The DME-UP case has a higher standard deviation, but the overall trend still matches each other.

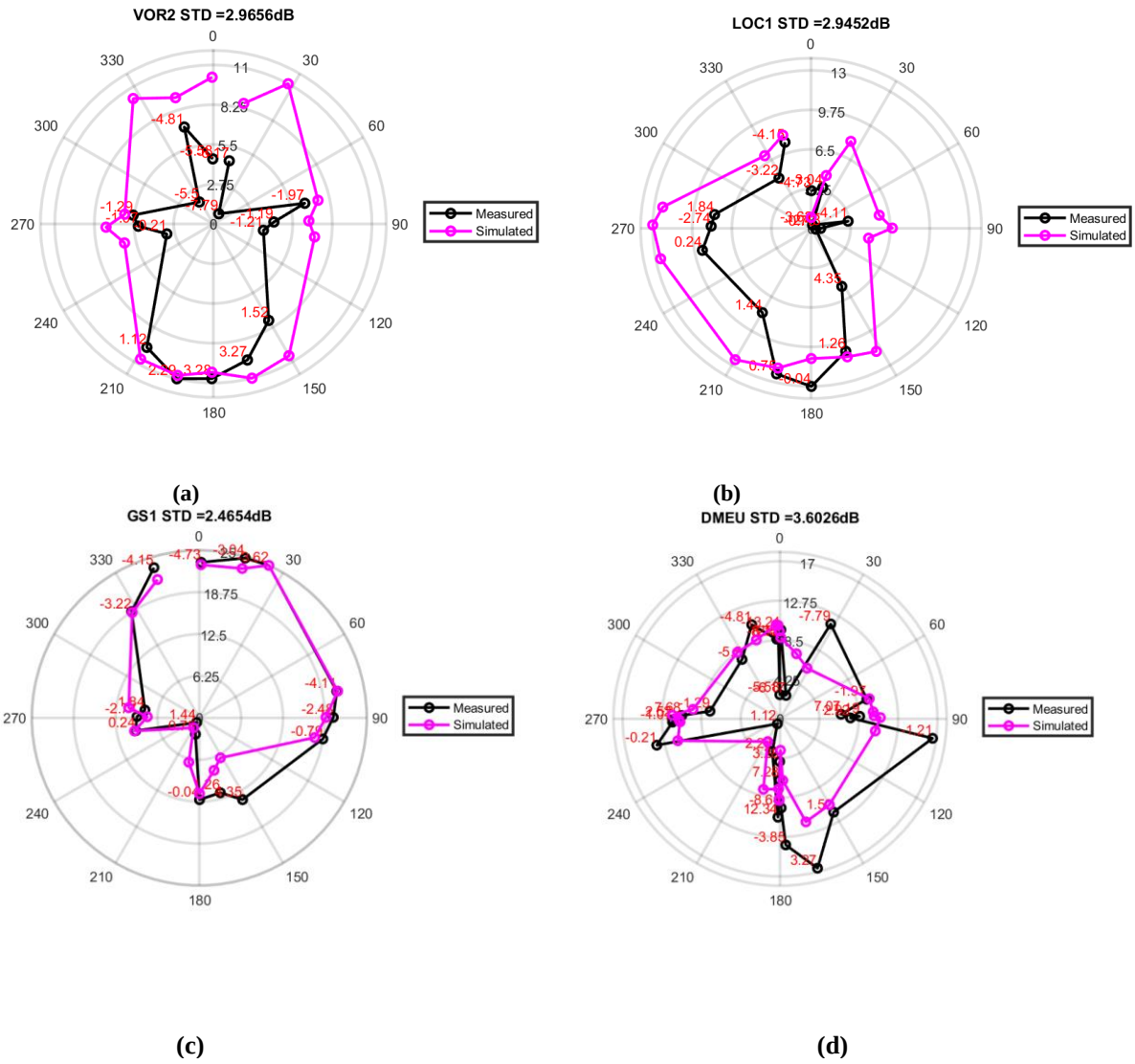

Figure 9: Comparing the unsmoothed EM simulation output with flight test measurement for the high-resolution measurement data, at specific measurement frequencies and in the aircraft coordinates (for "in flight" configuration). Data available is for King Air only. (a) VOR2 pattern at 108 MHz, (b) LOC1 pattern at 108 MHz, (c) GS1 pattern at 334.7 MHz, (d) DME-Upper pattern at 1155 MHz.

5. FURTHER WORK

This study is the initial investigation of combining CEM with flight data collection for the validation of navigational flight inspection. The technology and procedure can be applied to transponder and radar antenna systems and different flight platforms. Much more work is needed to achieve the final goal of precise validation of 3 dB SS accuracy in the field, while the initial validation shows some promise to it.

The simulation procedures, for example, will be applied to a platform based on small UAS, like the design shown in Figure 10. The hardware will be extremely low SWaP (as the payload of the UAS), with better supporting of omnidirectional probe antenna designs. The calibration data can be loaded into the onboard embedded computer so the flight inspection can be done in much faster speed than current solutions. More investigations are going on regarding the stability and accuracy of the SDR receivers that enable such capabilities.

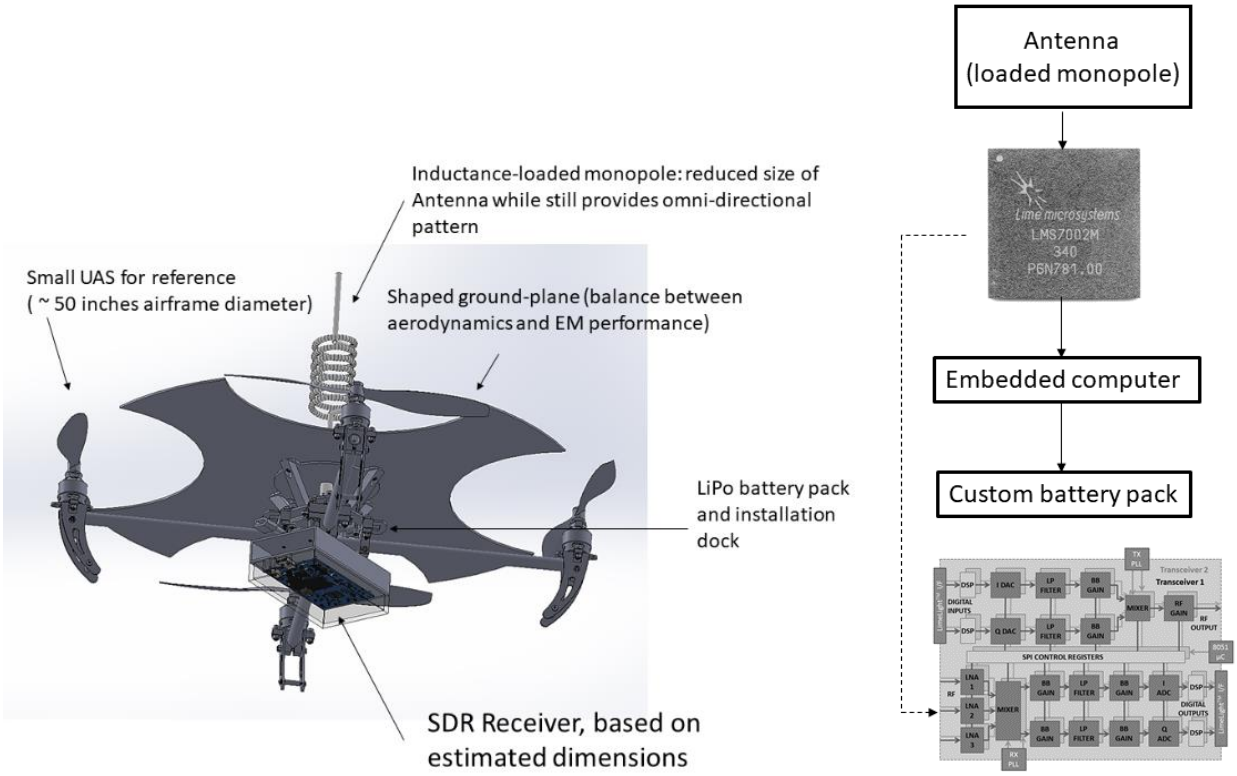

Figure 10: Concept design of the new UAS-based probing platform with SDR. LEFT: the UAS payload with antenna, RIGHT: the SDR system-on-chip architecture.

REFERRNCES

[1] FAA Navigation Programs, Transition Programs, VOR MON Program Page https://www.faa.gov/about/office_org/headquarters_offices/ato/service_units/techops/navservices (accessed 3/30/2018)

[2] Joint Committee for Guides in Metrology, 2010, Evaluation of measurement data – Guide to the expression of uncertainty in measurement, Corrected version 2010.

[3] ICAO, 31 October 2002, Manual On Testing of Radio Navigational Aids, Doc 8071, Volume 1, Testing of Ground-Based Radio Navigation Systems, 4th Edition.

[4] F. J. Jiménez, M. A. Sendarrubias, J. A. R. Moreno and E. P. Gil, "Modern electromagnetic simulation tools applied to On-aircraft Antenna Integration," *2012 6th European Conference on Antennas and Propagation (EUCAP)*, Prague, 2012, pp. 912-916. doi: 10.1109/EuCAP.2012.6205953

[5] A. Thain *et al*., "Numerical Modelling of Aircraft Antenna Installations," *The Second European Conference on Antennas and Propagation, EuCAP 2007*, Edinburgh, 2007, pp. 1-6. doi: 10.1049/ic.2007.0853

[6] https://core.ac.uk/download/pdf/26751773.pdf

[7] https://www.ion.org/ifis/abstracts.cfm?paperID=5610

[8] K. Horapong, D. Chandrucka, N. Montree and P. Buaon, "Design and use of "Drone" to support the radio navigation aids flight inspection," *2017 IEEE/AIAA 36th Digital Avionics Systems Conference (DASC)*, St. Petersburg, FL, 2017, pp. 1-6. doi: 10.1109/DASC.2017.8102114